Neural Computing and Applications (2024) 36:365–383
https://doi.org/10.1007/s00521-023-09010-0

ORIGINAL ARTICLE

Prediction of daily average seawater temperature using data-driven and deep learning algorithms

Arif Ozbek[1]

Received: 6 July 2022 / Accepted: 5 September 2023 / Published online: 4 October 2023
© The Author(s), under exclusive licence to Springer-Verlag London Ltd., part of Springer Nature 2023

Abstract

Large amounts of cooling water are required for the cooling process in coal-fired or nuclear power plants. Because the primary use of water in a power plant is to condense steam and remove waste heat as part of a Rankine cycle, seawater temperature (SWT) is of critical importance for electrical output in power plant applications installed at the seaside. Moreover, the analysis of SWT is an important criterion for researching sea life and global climate, and it also serves as an important indicator of climate change. In this paper, multilayer perceptron, which is in the class of a feed-forward artificial neural network, deep learning approach based on long short-term memory and bidirectional long short-term memory neural networks and data-driven methods, such as adaptive neuro-fuzzy inference system (ANFIS) accompanied by fuzzy c-means, ANFIS with grid partition and ANFIS with subtractive clustering methods were applied to make 1-day ahead SWT predictions. Analyses were conducted using 5-year daily mean SWTs measured by the Turkish State Meteorological Service for Antalya province between 2014 and 2018. The models were evaluated using mean absolute error (MAE), root-mean-square error (RMSE), and correlation coefficient (R). According to the daily SWT prediction, the best MAE, RMSE, and R values were obtained with the ANFIS-SC model, which were 0.1877 °C, 0.2683 °C, and 0.99814, respectively.

Keywords Seawater temperature · MLP · LSTM · BiLSTM · ANFIS-FCM · ANFIS-SC

1 Introduction

Since turbine efficiency in nuclear or coal power plants is directly dependent on seawater temperature, the turbine will run more efficiently when cooled with cold water. Therefore, although the reactor produces the same amount of energy throughout the year, electricity production will be at its highest in winter due to the lower water temperature [1]. Teguh et al. [2] presented a model for a steam power plant system to investigate the effect of the variation of the SWT on the performance of the steam power plant. Their model showed whether the power plant could achieve the required power output when there was a significant change in SWT. Huang et al. [3] reported that the thermal discharge from coastal nuclear power plants and thermal power plants increases the water temperature and also stratifies the seawater.

Machine Learning is the study of computer algorithms that improve themselves automatically via experience. Many studies have been conducted to estimate some meteorological and other parameters utilizing machine learning, data-driven and time series methods (see Table 1).

Several approaches for predicting sea surface temperature (SST) have recently been developed. Physical and statistical theories are the two main types of prediction models. The sea surface temperature is described using differential equation series in a physical model that aims at the physical properties of the ocean. Time series-based approaches for predicting sea surface temperature include statistical models that include linear regression and artificial neural networks (ANN). A model that uses artificial neural networks to estimate daily sea surface temperatures was described by Aparna et al. [29]. The predicted inaccuracy was less than 0.5 °C. Xuan et al. [19] proposed a sea surface temperature prediction model integrated with Deep

✉ Arif Ozbek
arozbek@cu.edu.tr

[1] Department of Mechanical Engineering, Ceyhan Engineering Faculty, Cukurova University, 01950 Adana, Turkey

Table 1 Summary of past research studies on machine learning methods and prediction parameters used in the literature

References	Method used	Prediction parameter
Kisi and Shiri [4]	Feed-forward ANN	Monthly air temperature
Bilgili and Sahin [5]	MLP	Monthly air temperature
Zaytar and El Amrani [6]	LSTM	Hourly air temperature
Tran et al. [7]	Traditional ANN, RNN, LSTM	Daily maximum air temperature
Roy [8]	MLP, LSTM, CNN + LSTM	Average air temperature
Ceylan [9]	GPR SVR, MLR	Agricultural energy consumption
Kaytez [10]	ARIMA-Least square SVM	Net electricity consumption
Qing and Niu [11]	LSTM	Solar irradiance
Ozbek et al. [12]	LSTM, ANFIS-FCM, ANFIS-GP	Energy production
Ozbek et al. [13]	LSTM, ANFIS-FCM, ARMA	Atmospheric air temperature
Balluf et al. [14]	LSTM	Wind speed
Qu et al. [15]	LSTM	Wind turbine power
Kisi and Sanikhani [16]	ANFIS-GP, ANFIS-SC	Atmospheric air temperature
Zhang et al. [17]	LSTM	Dam displacement
Peng et al. [18]	LSTM	Electricity price
Xuan et al. [19]	CNN network	Sea surface temperature
Pravallika et al. [20]	LSTM	Sea surface temperature
Sarkar et al. [21]	LSTM	Sea surface temperature
Graf and Aghelpour [22]	GMDH, ANFIS, RBF, AR, MA, ARMA, ARIMA	River water temperature
Zhu et al. [23]	FFNN, GPR	Daily river water temperature
Zhu et al. [24]	ANFIS-GP, ANFIS-SC, ANFIS-FCM, MLPNN	Daily river water temperature
Read et al. [25]	PGDL	Lake water temperature
Rajesh and Rehana [26]	SVR, KNN, RR, RF	River water temperature
Feigl et al. [27]	RNNs, FNNs, XGBoost	River water temperature
Kim and Jeong [28]	PGDL	Seawater temperature

Gated Recurrent Unit and Convolutional Neural Network (CNN network). CNN network's optimal architecture is configured using the Differential Evolution method. The accuracy of the prediction outcomes on the sea dataset was above 98% overall, and all mean absolute error (MAE) values were less than 0.33 °C. A recurrent neural network method named long short-term memory to estimate sea surface temperature using data from the previous year was presented by Pravallika et al. [20]. Haghbin et al. [30] presented a two-decade evaluation of soft computing model applications for forecasting sea surface temperature. The input variables, data sources, and performance indices for various models based on artificial neural networks, fuzzy logic, or other soft computing approaches, as well as input variables, data sources, and performance indices, were then discussed. Sarkar et al. [21] used a combination of deep learning neural networks and numerical estimators to make location-specific sea surface temperature predictions for daily, weekly, and monthly periods. Traditional neural networks were used to make predictions first, followed by deep learning networks. Over all periods and at all of the selected sites, the deep learning long short-term memory (LSTM) neural network improved its neural network model.

There are not many types of research in the literature that determine the estimation of seawater temperature (SWT) when compared to studies on sea surface temperature (SST) using machine learning approaches. Two numerical models for predicting river water temperature were suggested by Graf and Aghelpour [22]. Among the models used were the type-group method of data handling (GMDH), adaptive neuro-fuzzy inference system (ANFIS), radial basis function (RBF), stochastic type—autoregressive (AR), moving average (MA), autoregressive moving average (ARMA), and an autoregressive integrated moving average (ARIMA). Durmayaz and Sogut [31] and Kim and Yeong [28] examined cooling water temperature's effect on the thermal efficiency of the nuclear power station. They asserted that SWT has a direct impact on power plant efficiency. The hybrid Process Guided Deep Learning (PGDL) model was presented by Read et al. [25] to predict lake water temperatures. The RMSE value of 1.65 °C was

achieved using this model for temperature calculations in several lakes. The implementation of the hybrid model improved the prediction of critical environmental factors, according to this study. To estimate the temperature of the river, Stajkowski et al. [32] improved a genetic algorithm (GA)-optimized long short-term memory (LSTM) approach. The proposed hybrid time series regression model for forecasting utilized hourly water temperature data. Zhu et al. [23] built decision tree (DT), feed-forward neural network (FFNN), and Gaussian process regression (GPR) models to estimate daily river water temperature utilizing inputs such as the year, flow discharge, and air temperature. Their models were then tested in several river systems, and the results were compared to those of other models. Samadianfard et al. [33] used computational approaches such as adaptive neuro-fuzzy inference system (ANFIS), gene expression programming (GEP), and artificial neural networks to estimate the hourly water temperature at different depths in a lake in their nation. Three separate statistical measures (the root-mean-square error (RMSE), the mean absolute error (MAE), and the coefficient of correlation (R)) were used to evaluate the performance of their computing processes. To simulate daily water temperature in the river, Zhu et al. [24] used four different machine learning models: adaptive neuro-fuzzy inference systems (ANFIS) with grid partition method (ANFIS-GP), ANFIS with subtractive clustering method (ANFIS-SC), ANFIS with fuzzy c-mean clustering algorithm (ANFIS-FCM), and multilayer perceptron neural network models (MLPNN). The models they proposed were subsequently tested in a variety of river systems with various hydrological conditions. Quan et al. [34] refined a model for predicting reservoir water temperature by using solar radiation to assess and evaluate the water temperature of massive high-altitude reservoirs. Both the heuristic genetic algorithm (GA) and the support vector regression (SVR) approaches are used in their model. Attia [35] focused on the impact of cooling water temperature on a nuclear power plant's thermal performance. He demonstrated that the nuclear power plant's electricity generation and thermal efficiency declined by 0.444% and 0.152%, respectively, with just 1 °C increase in seawater temperature. Darmawan and Yuwono [36] examined the impact of changing the temperature of the seawater used as a condenser cooling medium on the steam turbine's performance. Feigl et al. [27] used six machine learning models to predict daily stream water temperature: two types of recurrent neural networks (RNNs), eXtreme Gradient Boosting (XGBoost), and feed-forward neural networks (FNNs), step-wise linear regression, and random forest. Many climate variables and their combinations were employed as model inputs. Hey-Min et al. [37] presented a deep learning-based approach to determine the occurrences of abnormally high water temperature events using the long short-term memory (LSTM) model. In their model, they used seawater temperatures from the previous ten years. Rajesh and Rehana [26] used new machine learning algorithms such as support vector regression (SVR), K-nearest neighbors (KNN) regressor, ridge regression (RR), and random forest (RF) regressor to predict river water temperature. Furthermore, the suggested machine learning algorithms were combined with the Ensemble Kalman Filter (EnKF) data assimilation (DA) approach to improve the accuracy of anticipated values based on measured data.

In this study, data-driven approaches and deep learning algorithms were developed to estimate 1-day-ahead SWT. SWT values were estimated using solely recorded SWT data, eliminating the necessity for different input parameters. Furthermore, the model with the highest sensitive results was determined. As a result, engineers and academics can use the study's findings to improve power plant modeling and planning.

2 Research significance and novelty of the study

Data-driven methods such as MLP, ANFIS-FCM, ANFIS-GP, ANFIS-SC, and deep learning algorithms based on LSTM and BiLSTM neural networks were proposed in this study to estimate 1-day-ahead seawater temperature from any measurement station. The followings are the most significant advances to the literature made by the study:

- The main benefit of the proposed models is that they can accurately estimate SWT values using only recorded seawater temperature data, without the need for different input parameters. For precise prediction, these methods rely on no geographic or meteorological information.
- To determine which of the models employed in this study produces more sensitive results, the results from all approaches using the same data sets were compared.
- The methods' output was evaluated and examined about varying input variables such as epoch number, hidden layer number, and influence radius.
- The prediction of SWT values over time series using data-driven and deep learning techniques, which has just recently been studied in a small number of papers.
- Selecting the most accurate method by comparing the most effective combinations of data-driven and deep learning methods.

As a result, it is hoped that this study will bridge a knowledge gap and significantly advance the subject.

3 Material and method

3.1 Methods

3.1.1 Multilayer perceptron (MLP)

The MLP network is a feed-forward approach that can be used to recreate hypersurfaces, mapping a set of multi-dimensional input data (x_i; $i = 1, \ldots, N$) onto a set of suitable multi-dimensional outputs (y_i; $i = 1\ldots, N$). The MLP architecture, which consists of one input layer, one or more hidden layer(s), and one output layer, has been widely employed in static regression applications. Back-propagation is a supervised learning technique used by the MLP network to train the network [38, 39].

Figure 1a depicts a schematic of the MLP neuron combination, whereas Fig. 1b illustrates a schematic layout of the single-layer MLP.

3.1.2 Long short-term memory (LSTM)

Hochreiter and Schmidhuber [40] were the first to introduce the LSTM approach. LSTM is a type of RNN that generates solutions by establishing cell states or memory cells with recurrent errors, allowing the faults to be reproduced without vanishing gradients. The LSTM contains three distinct gates. An input gate learns how to protect the memory cell's continuous error flow from unrelated inputs, an output gate learns how to protect other units from the memory cell's irrelevant memory content, and a forget gate, on the other hand, learns how to determine how long the values in the memory cell are stored [41, 42].

Following that, the data is split into two categories: training data and testing data. The first is used to model, while the second is utilized to validate the model. Parameters like batch size, learning rate, number of hidden layers, and maximum epoch may be assigned algorithmically or at random. To reach the predicted error target or maximum epoch, the gate function is computed and executed [41–44]. The LSTM layer design is depicted in Fig. 2, which displays the stream of an X time series with S-length C characteristics (channels) passing through an LSTM layer. The cell state is c_t, and the output is h_t at time step t, as indicated in the diagram. The initial LSTM section is used to evaluate the first output and the updated cell state for the

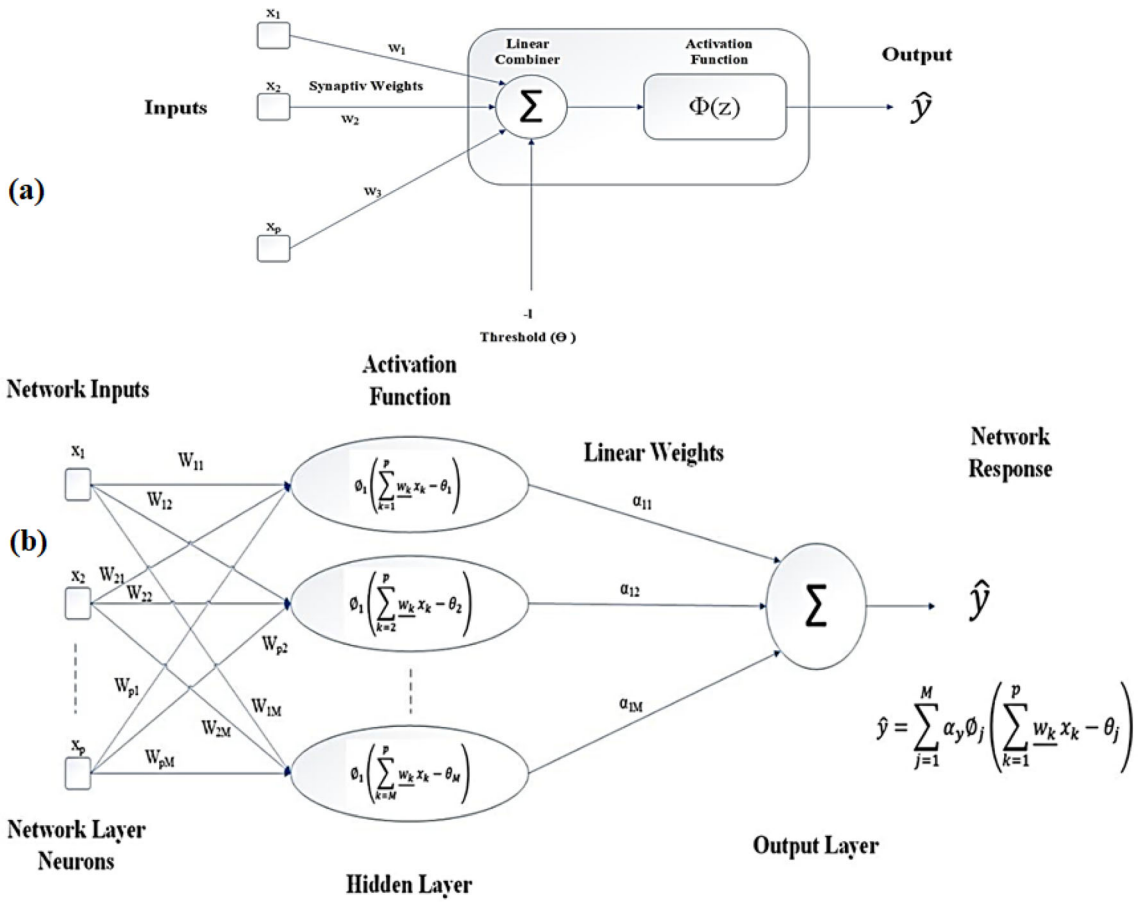

Fig. 1 Schematic display of MLP neuron (**a**), the flowchart of typical single line hidden layer MLP for identifying a problem (**b**) [39]

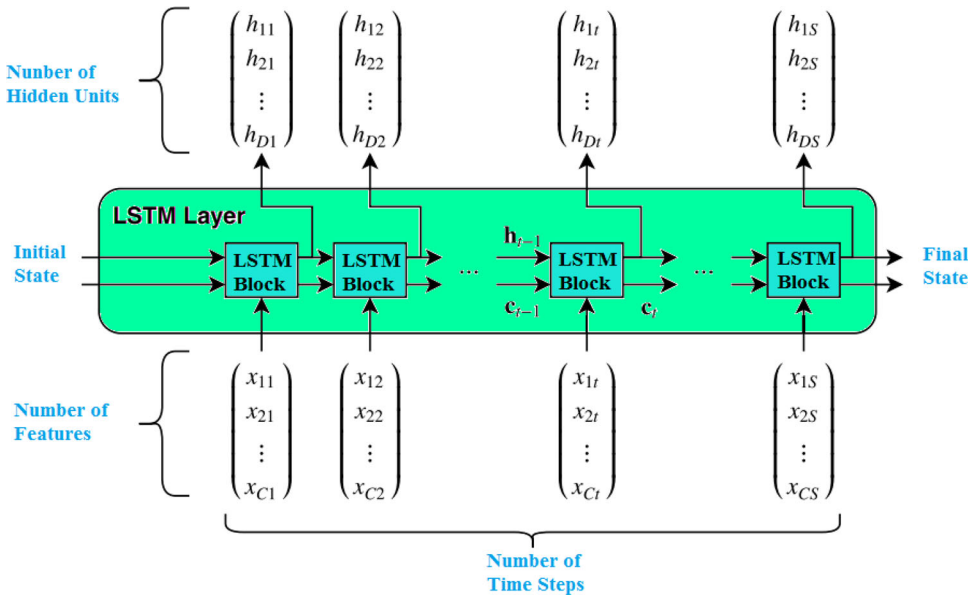

Fig. 2 The architecture of the LSTM layer [12]

network's first state and the series' first time step. This block calculates the updated cell state c_t and the output at time step t using the next time steps of the sequence and the network's up-to-date character (c_{t-1}, h_{t-1}).

The hidden state is the state of the layers, which includes the cell state. The outcome of the LSTM layers for this time step is incorporated in the concealed state at time step t. The information generated from the previous time step is stored in the cell state. The layer conducts the process of adding or removing information from the cell state at each time step. Gates was accustomed to reviewing these updates. The hidden state of the layers and cell state is controlled by several of the LSTM layer architecture's components. The level of cell state update and the level of cell state added to the hidden state, for example, are controlled by input I and output (o). The cell state reset level is checked by the forget gate (*forget*). Cell candidate (g), adds the information to the cell state.

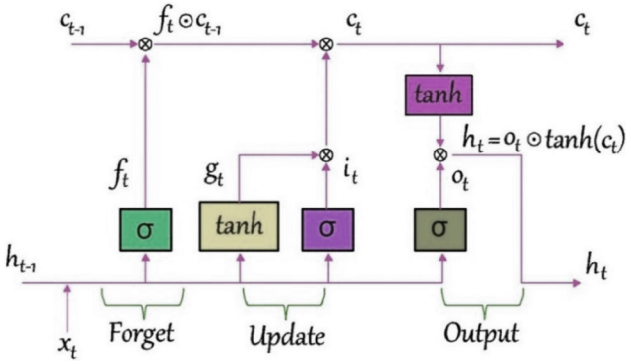

Fig. 3 The data flow at time step t [12]

The data migration at time step t is depicted in Fig. 3. The hidden states and cells are updated, forgotten, and output in this diagram.

LSTM layer weights that can be learned are the recurrent weights R, the input weights W, and the bias b. The matrices R, W, and b represent recurrent weights, component bias, and input weight concatenation, respectively. The following is how these matrices are concatenated:

$$R = \begin{bmatrix} R_i \\ R_f \\ R_g \\ R_o \end{bmatrix}, W = \begin{bmatrix} W_i \\ W_f \\ W_g \\ W_o \end{bmatrix}, b = \begin{bmatrix} b_i \\ b_f \\ b_g \\ b_o \end{bmatrix} \tag{1}$$

where the forget gate is f, the input gate is i, the cell candidate is g and the output is gate o. At the time step, the cell state t is indicated as,

$$c_t = f_t \odot c_{t-1} + i_t \odot g_t \tag{2}$$

where $\odot$ is the Hadamard product. At time step t, the hidden state is given by,

$$h_t = o_t \odot \tanh(c_t) \tag{3}$$

By default, the state activation function for the LSTM layer function is computed using the hyperbolic tangent function. At time step t, the following formulas explain the components [44]:

$$i_t = \sigma(R_i h_{t-1} + W_i x_t + b_i) \tag{4}$$

$$f_t = \sigma\left(R_f h_{t-1} + W_f x_t + b_f\right) \tag{5}$$

$$g_t = \tanh\left(R_g h_{t-1} + W_g x_t + b_g\right) \tag{6}$$

$$o_t = \sigma(R_o h_{t-1} + W_o x_t + b_o) \quad (7)$$

where σ is the gate activation function. The gate activation function is computed by the LSTM layer function using the sigmoid function, which is given by

$$\sigma(x) = (1 + e^{-x})^{-1} \quad (8)$$

3.1.3 Bidirectional long short-term memory (BiLSTM)

The BiLSTM model is a hybrid of the Bidirectional RNN (BiRNN) and the LSTM models. The BiRNN was introduced in 1997 by Schuster and Paliwal [45] for the first time. The BiRNN combines two RNN architectures, particularly forward and backwards RNNs. The RNN architecture is substituted with the LSTM architecture in the BiLSTM model to overcome the RNN's disappearing and increasing gradient problem. Graves and Schmidhuber [46] later presented the BiLSTM approach in 2005.

Figure 4 depicts the architecture of the BiLSTM method. $\overrightarrow{H}_t$ and $\overleftarrow{H}_t$ characters were introduced to describe the architecture of the BiLSTM for forwarding and backward hidden states. The following formula is used to calculate these hidden states:

$$\overrightarrow{H}_t = A(X_t W_{xh}^{\text{forw}} + \overrightarrow{H}_{t-1} W_{hh}^{\text{forw}} + b_h^{\text{forw}}) \quad (9)$$

$$\overleftarrow{H}_t = A(X_t W_{xh}^{\text{back}} + \overleftarrow{H}_{t-1} W_{hh}^{\text{back}} + b_h^{\text{back}}) \quad (10)$$

where W_{xh}^{forw} and W_{xh}^{back} specify the weight values for forward and backward input X_t, respectively, whereas W_{hh}^{forw} and W_{hh}^{back} specify the weight values for the forward and backward hidden state $\overrightarrow{H}_{t-1}$ and $\overleftarrow{H}_{t-1}$. b_h^{forw} and b_h^{back} represent the bias value for the forward and backward states. The activation function for the hidden layer is represented by A. The hidden state H_t can be obtained by concatenating $\overrightarrow{H}_t$ and $\overleftarrow{H}_t$. Finally, the output state can be calculated using H_t using the following formula:

$$O_t = H_t W_o + b_o \quad (11)$$

where W_o and b_o are the weight and bias values in the output layer [47, 48].

3.1.4 Adaptive neuro-fuzzy inference system (ANFIS)

ANFIS is a global estimator. It can be used to execute any real linear function with any degree of precision in a small space. Essentially, ANFIS is a network model for Sugeno-type fuzzy systems with neural learning capabilities that use neural network learning methods to produce fuzzy if–then rules and suitable membership functions (MF) from input–output. The adaptive neural network framework for FIS development is abbreviated as ANFIS [49, 50]. Figure 5 displays the Type-3 fuzzy reasoning ANFIS architecture (Type-3 ANFIS) and its associated counterpart.

In general, there are two parts to an ANFIS model: construction and training. During the construction phase, the types and numbers of membership functions are provided, and the input–output data is separated into rule patches. With the use of the ANFIS model, clustering methods are used to understand and categorize inputs into groups, facilitating the training phase, which explains why three clustering approaches, including FCM, subtractive clustering (SC), and grid partitioning (GP), are used. More details on ANFIS were provided in [51–55].

3.2 Data sources

The measurement station is located in Antalya province in the south of Turkey as can be seen in Fig. 6. The SWT station's geographic coordinates are 36° 52′ 49.4″ N and 30° 40′ 54.6″ E. Analyzes were performed by using 5-year daily mean SWTs measured by the Turkish State Meteorological Service between 2014 and 2018 years at Antalya province (Fig. 7). The input data size in this study was 1825 daily mean SWT value. All of the daily

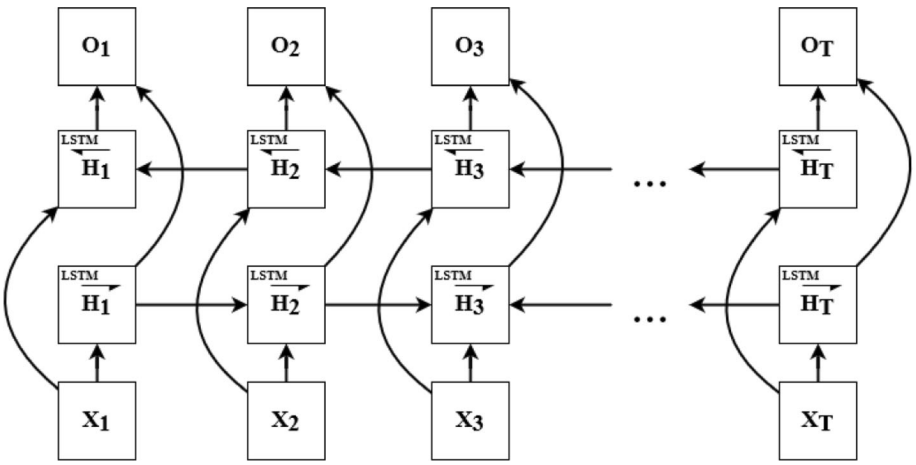

Fig. 4 Architecture of BiLSTM method [48]

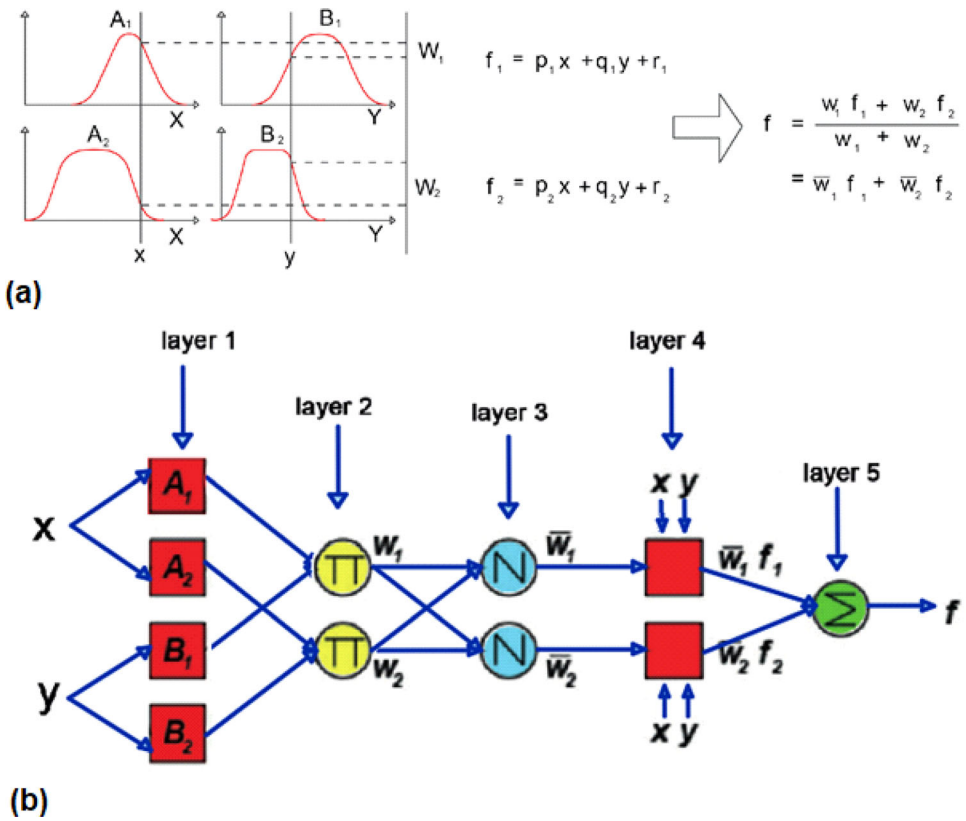

Fig. 5 Fuzzy reasoning of type 3 (**a**); ANFIS equivalent (Type-3 ANFIS) (**b**) [13]



Fig. 6 Location of the measurement station

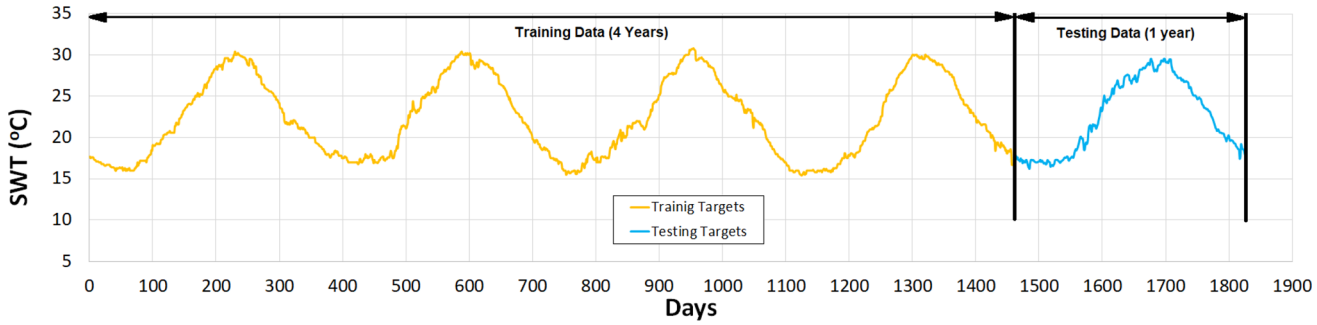

Fig. 7 Time series of the seawater temperature (SWT) in Antalya province

measurements were executed at 2 m below the sea surface using a PT100 type marine thermometer. From the measured data, the maximum, minimum and average SWT values are 30.8 °C, 15.4 °C and 22.3 °C, respectively, with a standard deviation of 4.7 °C.

Figure 7 also depicts the observed or target seawater temperature (SWT) values with 4 years of training and 1 year of testing data for the approaches. From 01 January 2014 to 31 December 2017, 1460 daily sample data (first four years and 80% of total data) were used to train the approach. From 01 January 2018 to 31 December 2018, 365 daily sample data (last year and 20% of total data) were used to test it. In the summary, models were trained using the first 1425 (4 years) of 1825 daily average seawater temperatures measured between 2014 and 2018, and 365 SWT values for the last 1 year (2018 year) were estimated.

The main flowchart of the suggested deep learning approaches for SWT prediction is depicted in Fig. 8. The simulation parameters were set after the SWT data from the seawater was supplied. After the data from the marine thermometer was collected, it was pre-processed and cleared for the following phase by deleting missing and outlier readings and imputing values. After that, the model was trained by adjusting simulation settings such as epoch number, hidden layer number, and influence radius. The prediction method was carried out utilizing the test data from the training model. The data was then normalized, and the predicted SWT values were derived. To assess the precision of the proposed model, various statistical measures such as MAE, RMSE, and R were used. Finally, the model developed was utilized to forecast SWT. The model was run using MATLAB R2018a (Trial Version).

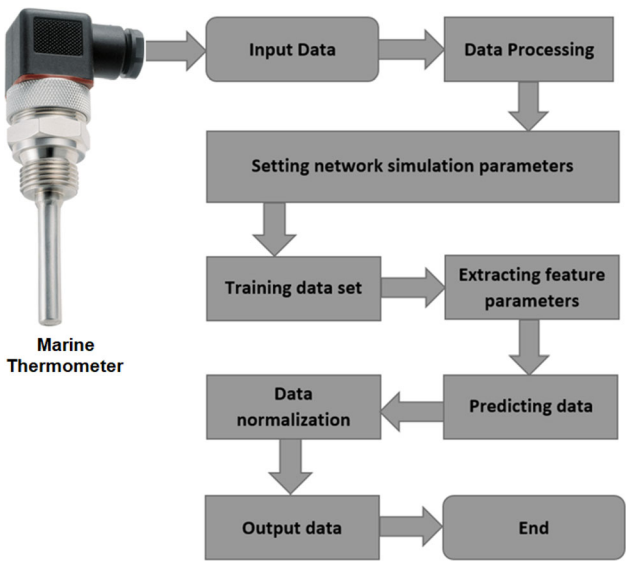

Fig. 8 Seawater temperature (SWT) prediction flowchart based on the deep learning models

3.3 Error analysis

Three statistical error criteria have been used in this study, which is shown by the abbreviations MAE, RMSE, and *R*, which correspond to mean absolute error (MAE), root mean square error (RMSE), and correlation coefficient (*R*), respectively. These error criteria were used to assess the accuracy of a model in predicting an observed (target) output variable, in this work. Their calculation methods are, respectively, provided as follows [12]:

$$\mathrm{MAE} = \frac{1}{N}\sum_{i=1}^{N}|p(i) - o(i)| \tag{12}$$

$$\mathrm{RMSE} = \sqrt{\frac{1}{N}\sum_{i=1}^{N}[p(i) - o(i)]^2} \tag{13}$$

$$R = \left(\sum_{i=1}^{N}[p(i) - \bar{p}][o(i) - \bar{o}]\right) \Big/ \left(\sqrt{\sum_{i=1}^{N}[p(i) - \bar{p}]^2}\sqrt{\sum_{i=1}^{N}[o(i) - \bar{o}]^2}\right) \tag{14}$$

In these equations, $p(i)$ designation and $o(i)$ assignment imply predicted values and target values at the time I, respectively. Beyond, the terms $\overline{p}$ and $\overline{o}$ represent the

averages of the predicted values and target values, respectively, when N represents the total number of data.

4 Result and discussion

4.1 Multilayer perceptron (MLP)

First, the MLP method was chosen, and various neuron and iteration numbers were utilized in the simulation. The MAE, RMSE, and R values were used to analyze the method's performance. Table 2 shows the simulation outcomes. The effect of the number of neurons and iteration number can easily be seen in the outcomes from that table. The best predictions were obtained when 5 input numbers, 6 neuron numbers, and 1000 iteration numbers were used. The use of a large number of neurons did not give satisfying outcomes. MAE is 0.1886 °C and RMSE is 0.2690 °C at the end of the simulation, with an R value of 0.99813.

The simulation results of the MLP model for the Antalya station are shown in Fig. 9a. This chart displays the targets and the predicted data between January 1st, 2018 and December 31st, 2018. Figure 9b depicts the target and predicted data difference. In December, the difference between the target and predicted SWT values reached a maximum of 1.5 °C. The histogram diagram of the target values for the SWT predictions is shown in Fig. 9c. As seen in this graph, the results of the MLP model for the Antalya station appear to be skewed to the positive, with more than 88% of the model predictions having an inaccuracy of 0.4 °C. Figure 9d depicts the regression graph of the target data versus the prediction. The X-axis and Y-axis of this figure denote the target or real and predicted values of the SWT data in the Celsius unit, respectively. The figure illustrates that the predicted data is of high quality and provides a good fit.

4.2 Long short-term memory (LSTM)

Table 3 shows the Antalya station's estimation of ideal parameters for SWT prediction using the LSTM approach. The best results are highlighted in bold in this table. To demonstrate the method's performance, MAE, RMSE, and R values were determined. This table indicates the significance of the hidden layer number and epoch number. The best result was obtained from 50 hidden layers and 500 epoch numbers. The lowest MAE and RMSE were obtained as 0.2594 °C and 0.3487 °C, respectively, with an R value of 0.99688. The MAE and RMSE values increased with a further increase in hidden layer numbers.

Figure 10a represents the target (blue) and predicted (red) testing SWT values for the Antalya station using the LSTM approach between 01 January 2018 and 31 December 2018. Figure 10b illustrates the difference between the target and predicted data. In April and December months, the measured and estimated SWT temperatures varied by 1.4 °C. The LSTM histogram plot of the predicted SWT values is shown in Fig. 10c. The results produced using this model in the Antalya station appear to be skewed to the positive. As can be seen in the graph, more than 81% of the model estimations have an error $\leq \pm 0.4$ °C. Figure 10d depicts the regression plot of the target and predicted data. The X-axis and Y-axis of this figure denote the target or real and predicted values of the SWT data in the Celsius unit, respectively. With an R value of 0.99688, the target and predicted data acquired by the LSTM technique closely match this station.

4.3 Bidirectional long short-term memory (BiLSTM)

Table 4 illustrates the results of predicting the hourly SWT using this approach. When two layers are utilized, the lowest MAE is 0.2880 °C and RMSE is 0.3871 °C with an R value of 0.99625. That method was employed using 50 units in both the first and the second layers and 500 epoch

Table 2 Daily SWT performance prediction for the MLP model (Best results are in bold)

Input number	Neuron number	Max iterations	MAE (°C)	RMSE (°C)	R
5	5	100	0.1952	0.2756	0.99785
5	5	500	0.1905	0.2728	0.99808
5	6	100	0.1912	0.2714	0.99846
5	6	500	0.1893	0.2702	0.99835
5	**6**	**1000**	**0.1886**	**0.2690**	**0.99813**
5	7	500	0.1919	0.2760	0.99826
5	7	1000	0.1909	0.2749	0.99821
5	8	1000	0.1926	0.2753	0.99825
5	9	1000	0.1985	0.2756	0.99824
5	10	1000	0.1943	0.2766	0.99827

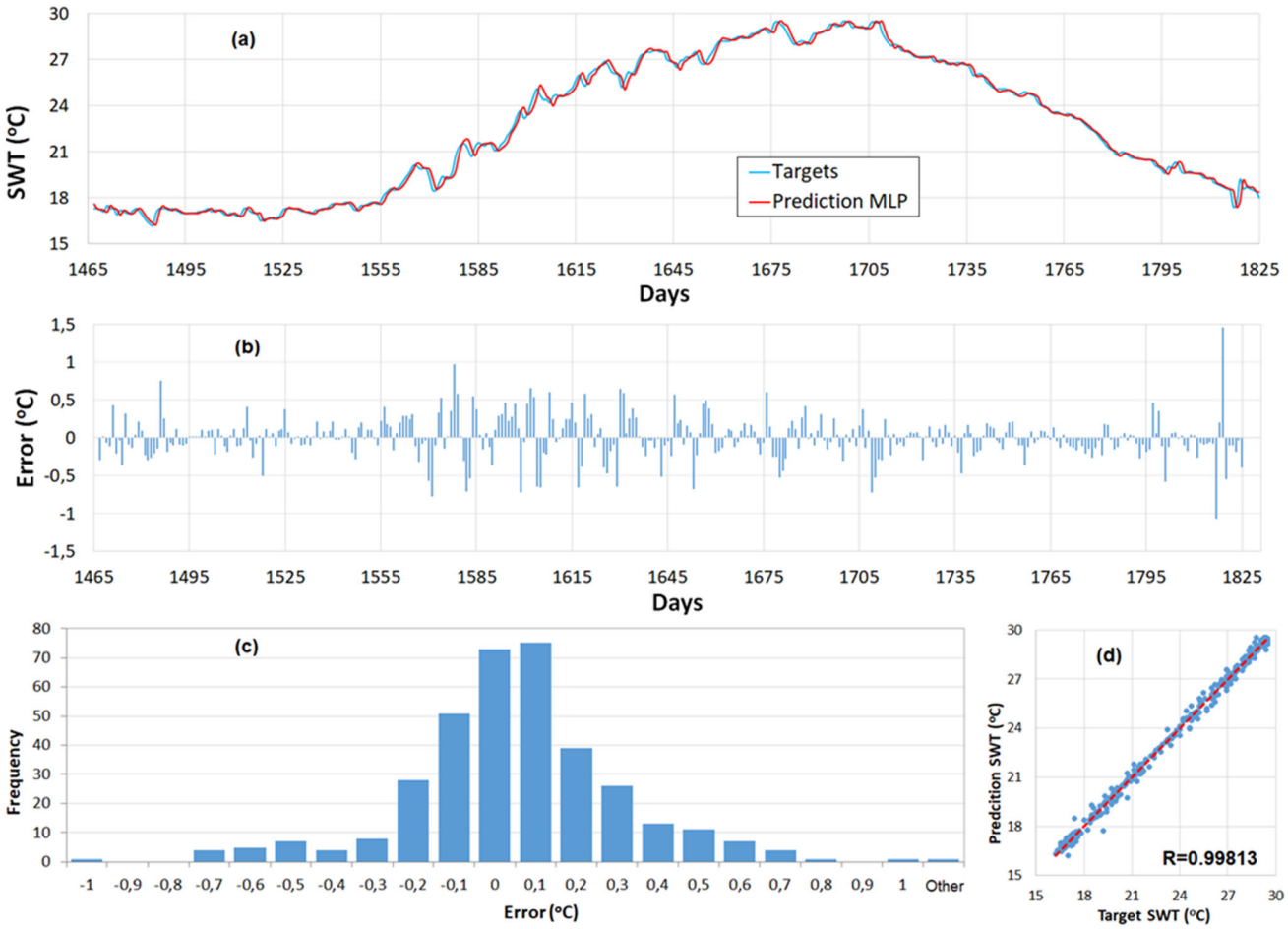

Fig. 9 Observed or target (blue) and predicted (red) testing SWT values (**a**), the difference between the target and the forecasted data (**b**), histogram of prediction errors for the model (**c**), regression plot of the target and the forecasted data (**d**) (color figure online)

Table 3 Daily SWT performance prediction for the LSTM model (Best results are in bold)

Hidden layer number	Epoch number	MAE (°C)	RMSE (°C)	*R*
5	100	0.2903	0.3678	0.99388
5	300	0.2872	0.3642	0.99414
10	300	0.2823	0.3598	0.99546
25	300	0.2746	0.3579	0.99512
50	300	0.2658	0.3532	0.99598
50	**500**	**0.2594**	**0.3487**	**0.99688**
100	300	0.2646	0.3513	0.99605
100	500	0.2675	0.3502	0.99612

numbers. It can also be noted that when using three or more layers does not seem to affect the results much.

The target (blue) and predicted (red) testing SWT values for the Antalya station using the BiLSTM method between 01 January 2018 and 31 December 2018 are shown in Fig. 11a. The difference between the target and predicted data is illustrated in Fig. 11b. The target and estimated SWT temperatures varied a maximum of 1.5 °C in April. The BiLSTM histogram plot of the predicted SWT values is shown in Fig. 11c. The results produced using this model in the station appear to be skewed to the positive. As can be seen in the graph, more than 81% of the model estimations have an error $\leq \pm 0.4$ °C. Figure 11d depicts the regression plot of the target and predicted data. The target and predicted data were obtained by the BiLSTM approach in this station with an *R* value of 0.99625.

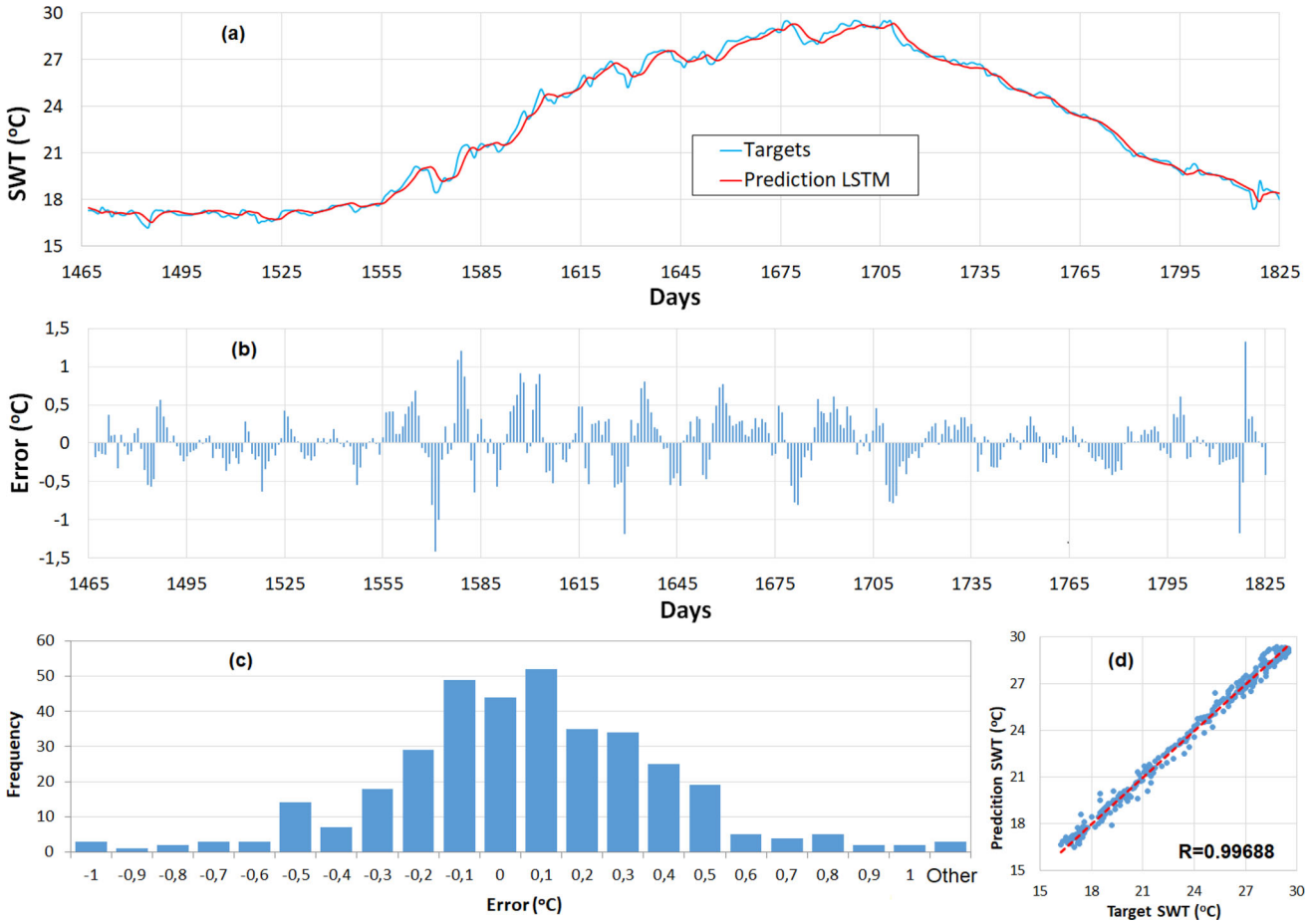

Fig. 10 Observed or target (blue) and predicted (red) testing SWT values (**a**), the difference between the target and the forecasted data (**b**), histogram of prediction errors for the model (**c**), regression plot of the target and the forecasted data (**d**) (color figure online)

Table 4 Daily SWT performance prediction for the BiLSTM model (Best results are in bold)

Number of layers	Units in first layer	Units in second layer	Epoch number	MAE (°C)	RMSE (°C)	*R*
2	5	5	100	0.3456	0.4258	0.98234
2	5	5	300	0.3345	0.4214	0.98862
2	5	5	500	0.3088	0.4101	0.99144
2	5	10	300	0.3225	0.4158	0.98997
2	5	20	300	0.3102	0.4156	0.99048
2	10	10	300	0.3024	0.4026	0.99199
2	20	20	300	0.2972	0.3969	0.99257
2	20	20	500	0.2903	0.3924	0.99363
2	20	20	700	0.2982	0.3931	0.99592
2	**50**	**50**	**500**	**0.2880**	**0.3871**	**0.99625**

4.4 Fuzzy C-means clustering (ANFIS-FCM)

Various clusters such as input and epoch numbers were used in the Fuzzy C-Means Clustering (ANFIS-FCM) model. The performance of the method was assessed by calculating MAE, RMSE and *R* values. The simulation results are represented in Table 5. From that table, the influence of the number of cluster nodes (membership functions = MFs) and fuzzy can be easily detected in the results. 2 clusters (MFs) are determined as the best one that

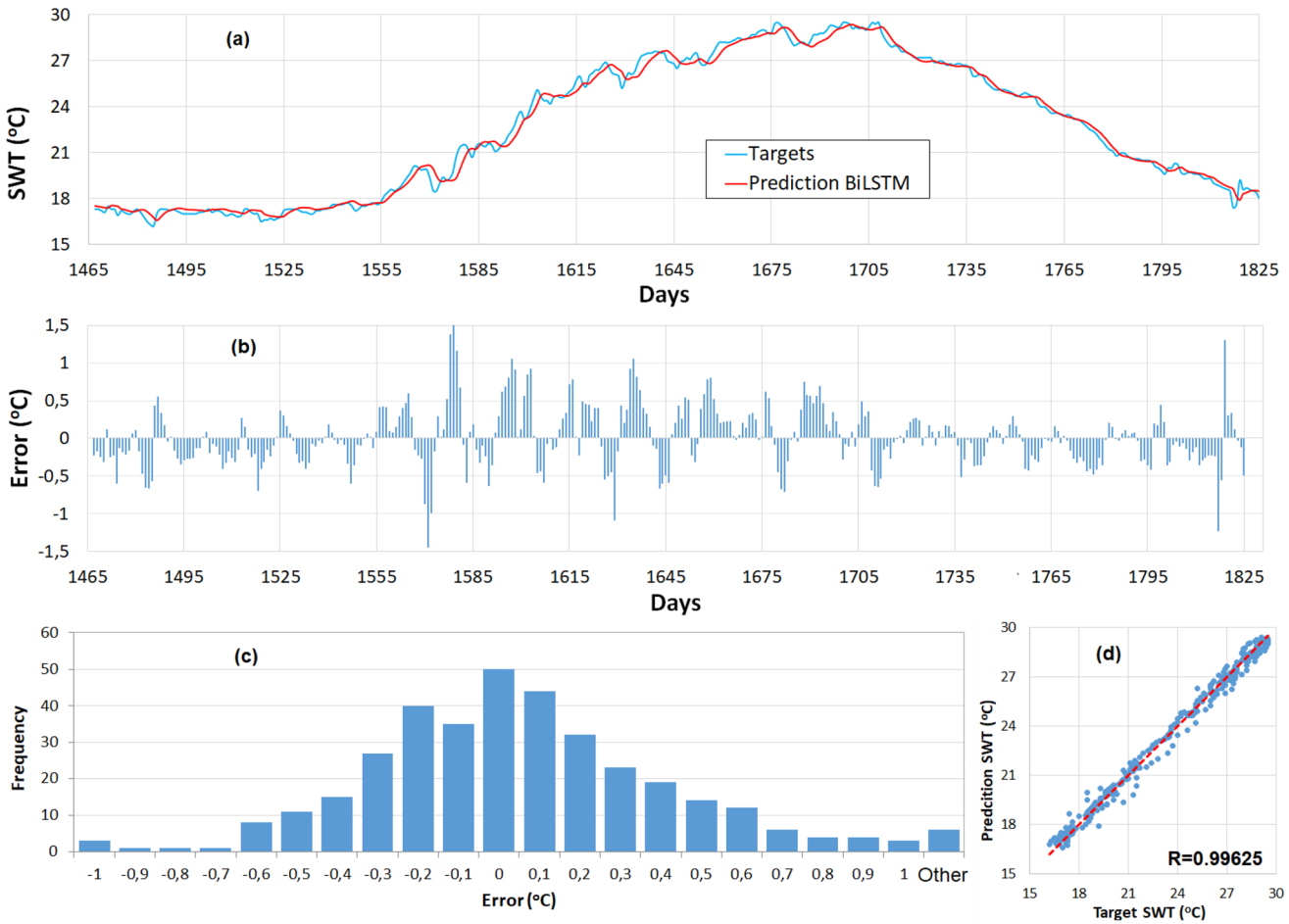

Fig. 11 Observed or target (blue) and predicted (red) testing SWT values (**a**), the difference between the target and the forecasted data (**b**), histogram of prediction errors for the model (**c**), regression plot of the target and the forecasted data (**d**) (color figure online)

Table 5 Daily SWT performance prediction for the ANFIS-FCM model (Best results are in bold)

Number of MFs	Input number	Max epoch	MAE (°C)	RMSE (°C)	*R*
2	5	100	0.2079	0.2874	0.99752
2	**5**	**300**	**0.1914**	**0.2741**	**0.99806**
2	5	500	0.2083	0.2886	0.99746
3	5	100	0.2095	0.2895	0.99740
3	5	300	0.2089	0.2882	0.99748
4	5	300	0.2097	0.2891	0.99642
5	5	300	0.2113	0.2946	0.99605
6	5	300	0.2110	0.2947	0.99605
7	5	300	0.2126	0.2969	0.99590
8	5	300	0.2152	0.2918	0.99558

uses 5 input numbers and 300 epoch numbers. A low number of clusters yield satisfactory results owing to the good separation of the inputs. Furthermore, an increasing number of clusters and smaller input numbers do not give a good solution. At the end of the simulation, MAE is 0.1914 °C and RMSE is 0.2741 °C with an *R* value of 0.99806.

For the station, the simulation outcomes of the ANFIS model using the FCM clustering model can be seen in Fig. 12a. From January 1, 2018, to December 31, 2018, this graph depicts not only observed but also predicted data. The difference between the target and estimated data is seen in Fig. 12b. The difference between the target and estimated SWT values reached 1.5 °C in December.

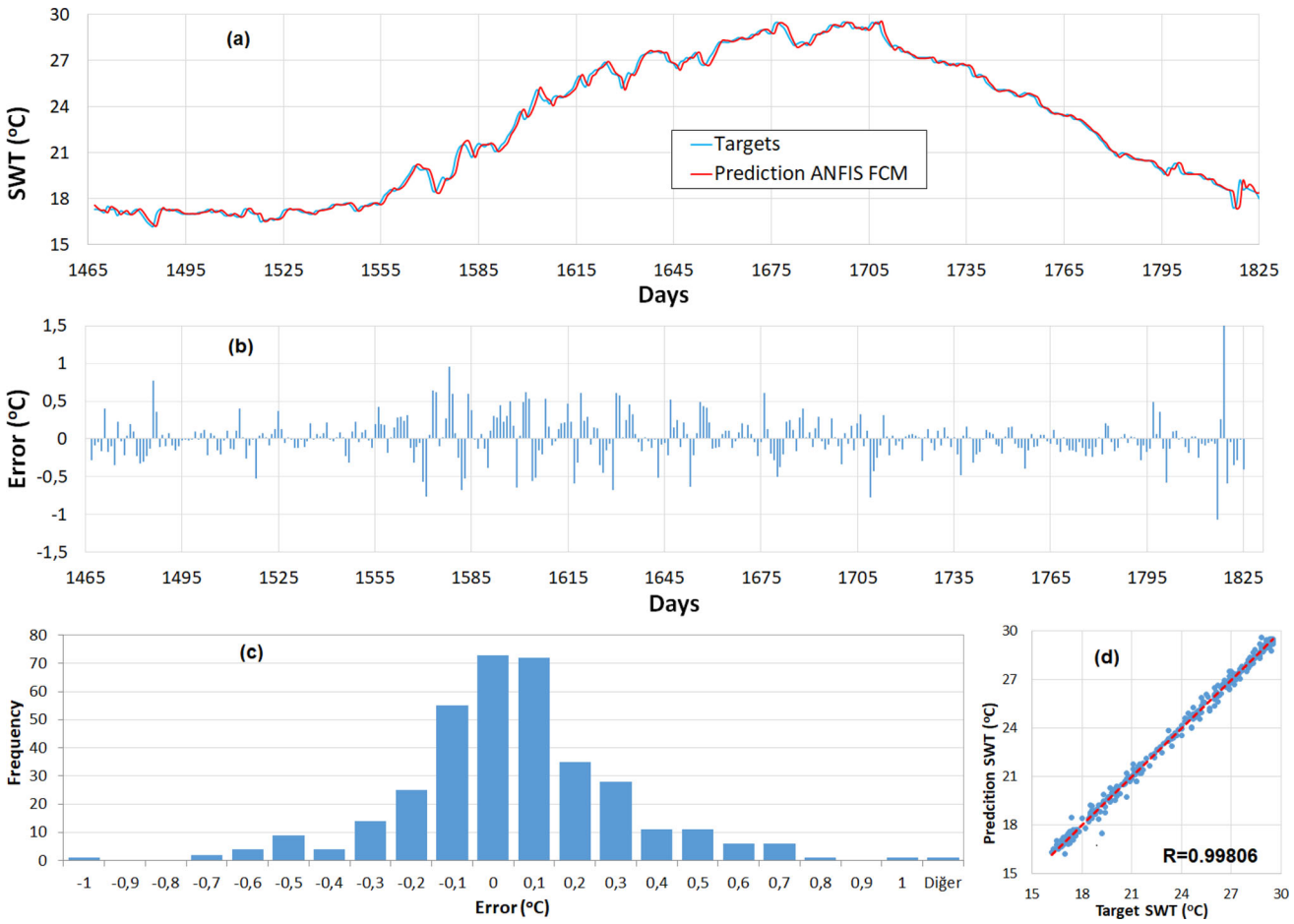

Fig. 12 Observed or target (blue) and predicted (red) testing SWT values (**a**), the difference between the target and the forecasted data (**b**), histogram of prediction errors for the model (**c**), regression plot of the target and the forecasted data (**d**) (color figure online)

Figure 12c shows a histogram graphic of the target values for the SWT predictions. The outcomes of the ANFIS-FCM approach for the Antalya station appear to be skewed to the positive, as shown in this graph, with more than 88% of the model predictions having a 0.4 °C error. The regression graph of the target data versus the prediction is shown in Fig. 12d. The model in this station obtained the target and predicted data with an R value of 0.99806.

4.5 Grid partitioning (ANFIS-GP)

Table 6 illustrates the outcomes of applying this classification model to forecast the daily SWT. When employing 2 clusters, 5 input numbers, and 10 epoch numbers, the lowest MAE is 0.1883 °C and the RMSE is 0.2696 °C with an R value of 0.99812. When two clusters and five input numbers are used, also raising the epoch number increases MAE and RMSE.

Table 6 Daily SWT performance prediction for the ANFIS-GP model (Best results are in bold)

Number of MFs	Input number	Max epoch	MAE (°C)	RMSE (°C)	R
2	**5**	**10**	**0.1883**	**0.2696**	**0.99812**
2	5	50	0.1929	0.2749	0.99787
2	5	100	0.1937	0.2825	0.99752
2	5	200	0.1975	0.2972	0.99744
2	6	50	0.1978	0.2866	0.99726
2	6	100	0.1974	0.2877	0.99717
2	7	100	0.2001	0.2655	0.99796

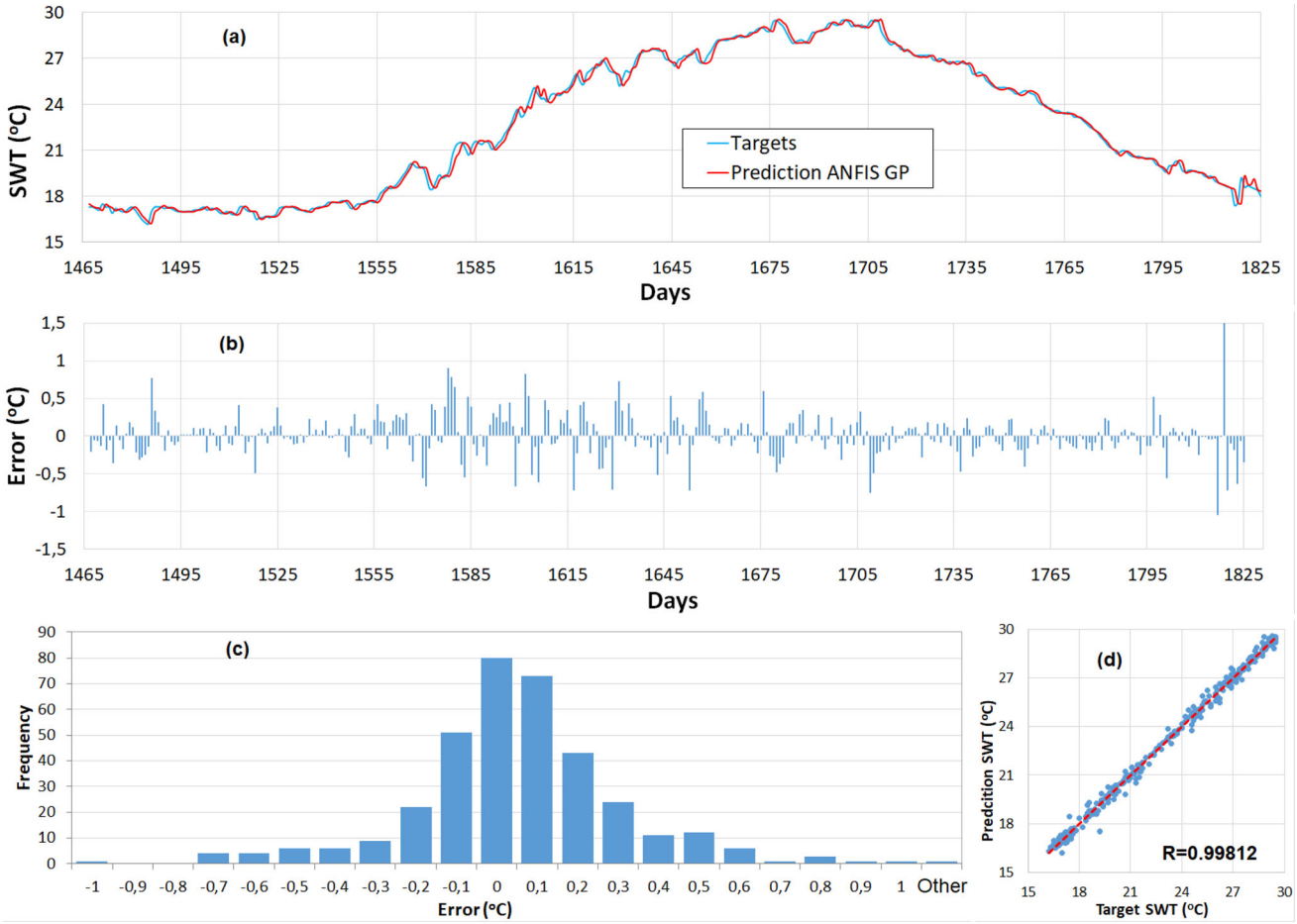

Fig. 13 Observed or target (blue) and predicted (red) testing SWT values (**a**), the difference between the target and the forecasted data (**b**), histogram of prediction errors for the model (**c**), regression plot of the target and the forecasted data (**d**) (color figure online)

Figure 13a represents the simulation results of the ANFIS model that makes use of the GP clustering model. In that figure, the target and the predicted data between 01 January 2018 and 31 December 2018 can be seen. Figure 13b depicts the error values between the target and forecasted data. In December, the difference between the target and forecasted SWT values reached a maximum of 1.5 °C temperature difference. The histogram diagram of the target values for the SWT predictions is represented in Fig. 13c. As can be seen from this figure, the outcomes of the ANFIS-FCM approach for the Antalya station appear to be skewed to the positive, with more than 88% of the model predictions having an inaccuracy of 0.4 °C. Figure 13d depicts the regression graph of the target data versus the prediction. The target and predicted data were obtained by the model in this station with an *R* value of 0.99812.

4.6 Subtractive clustering (ANFIS-SC)

Table 7 shows the results of various evaluation criteria for the ANFIS-SC model. In this regard, the applied prediction methodology was investigated utilizing this method for a variety of cluster radius sets, including ranges of $0.2 \leq R \leq 0.9$. Table 7 illustrates the outcomes of the ANFIS-SC model's estimation testing process. As the table shows, all of the examined ANFIS-SC models gave results that were nearly equal in terms of precision metrics. The radius of 0.7, on the other hand, has improved MAE, RMSE, and R statistics. The MAE, RMSE, and R statistics for that province at this radii value were 0.1877 °C, 0.2683 °C, and 0.99814, respectively.

The simulation results of the ANFIS model, which uses the SC clustering model, are shown in Fig. 14a. The target and forecasted data for the period 01 January 2018 to 31 December 2018 can be seen in that diagram. The error values between the target and forecasted data are shown in Fig. 14b. The temperature discrepancy between the target and predicted SWT values reached a high of 1.5 °C in

Table 7 Daily SWT performance prediction for the ANFIS-SC approach (Best results are in bold)

Influence radius (R)	Input Number	Max epoch	MAE (°C)	RMSE (°C)	R
0.2	5	300	0.1938	0.2888	0.99675
0.3	5	300	0.1994	0.2832	0.99711
0.4	5	300	0.1986	0.2794	0.99746
0.5	5	300	0.1994	0.2796	0.99737
0.6	5	300	0.1986	0.2788	0.99744
0.7	**5**	**300**	**0.1877**	**0.2683**	**0.99814**
0.8	5	300	0.1972	0.2768	0.99756
0.9	5	300	0.1974	0.2765	0.99753

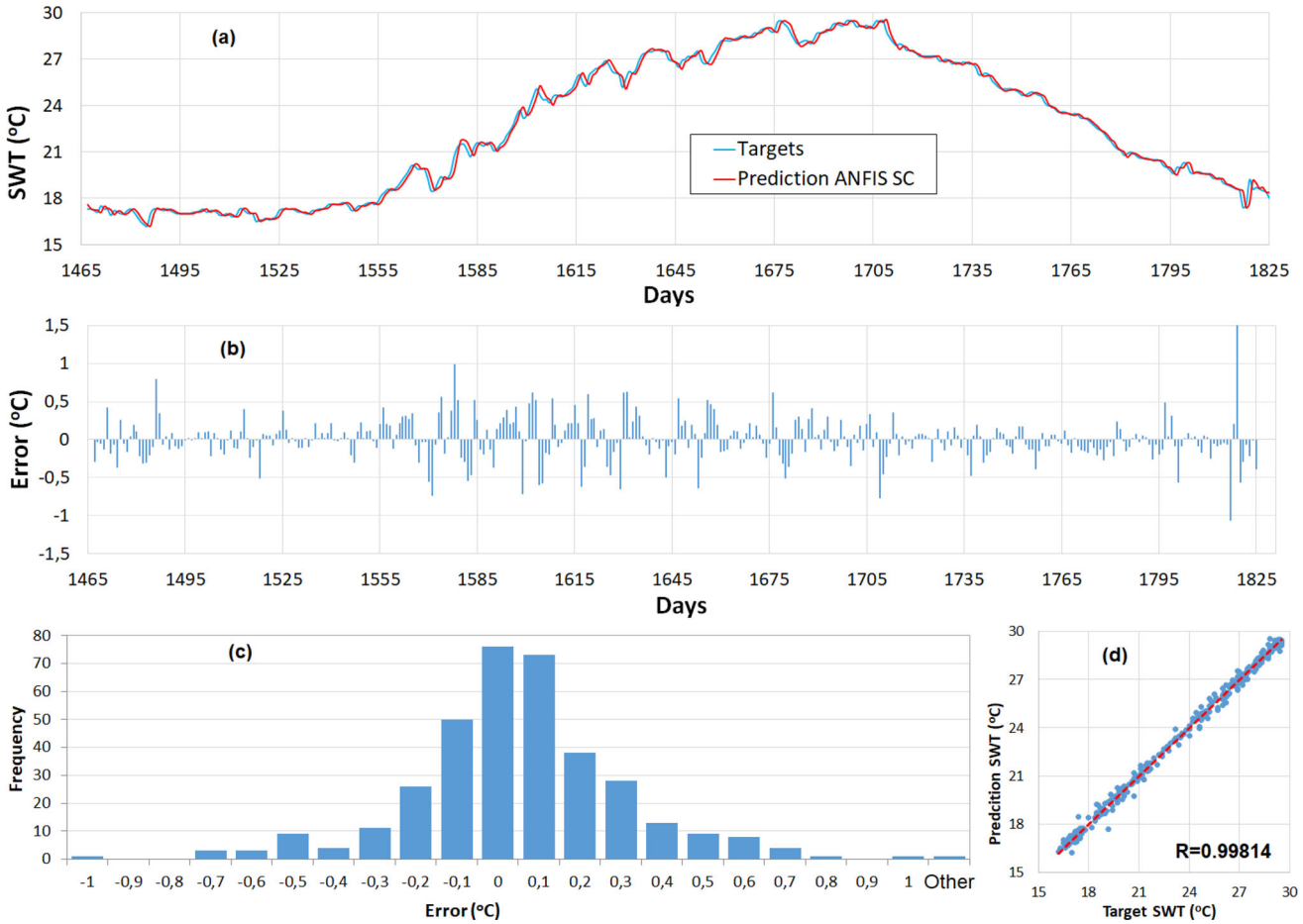

Fig. 14 Observed or target (blue) and predicted (red) testing SWT values (**a**), the difference between the target and the forecasted data (**b**), histogram of prediction errors for the model (**c**), regression plot of the target and the forecasted data (**d**) (color figure online)

December. Figure 14c shows a histogram graphic of the target values for the SWT forecasts. The outcomes of the ANFIS-FCM approach for the Antalya station appear to be skewed to the positive, with more than 88% of the model forecasts having an error of 0.4 °C, as can be seen in this figure. The regression graph of the target data versus the prediction is shown in Fig. 14d. The model in this station obtained the target and predicted data with an R value of 0.99814.

5 Comparison of the models

The purpose of the comparison was to evaluate which of the six approaches shown here was the most effective. Figure 15a–c illustrates the comparison of targets and predicted daily SWT values for different one-month periods between 1st–30th April, 1st–30th June, and 1st–31st December, respectively. The most successful combinations, as identified in Tables 2, 3, 4, 5, 6 and 7, were

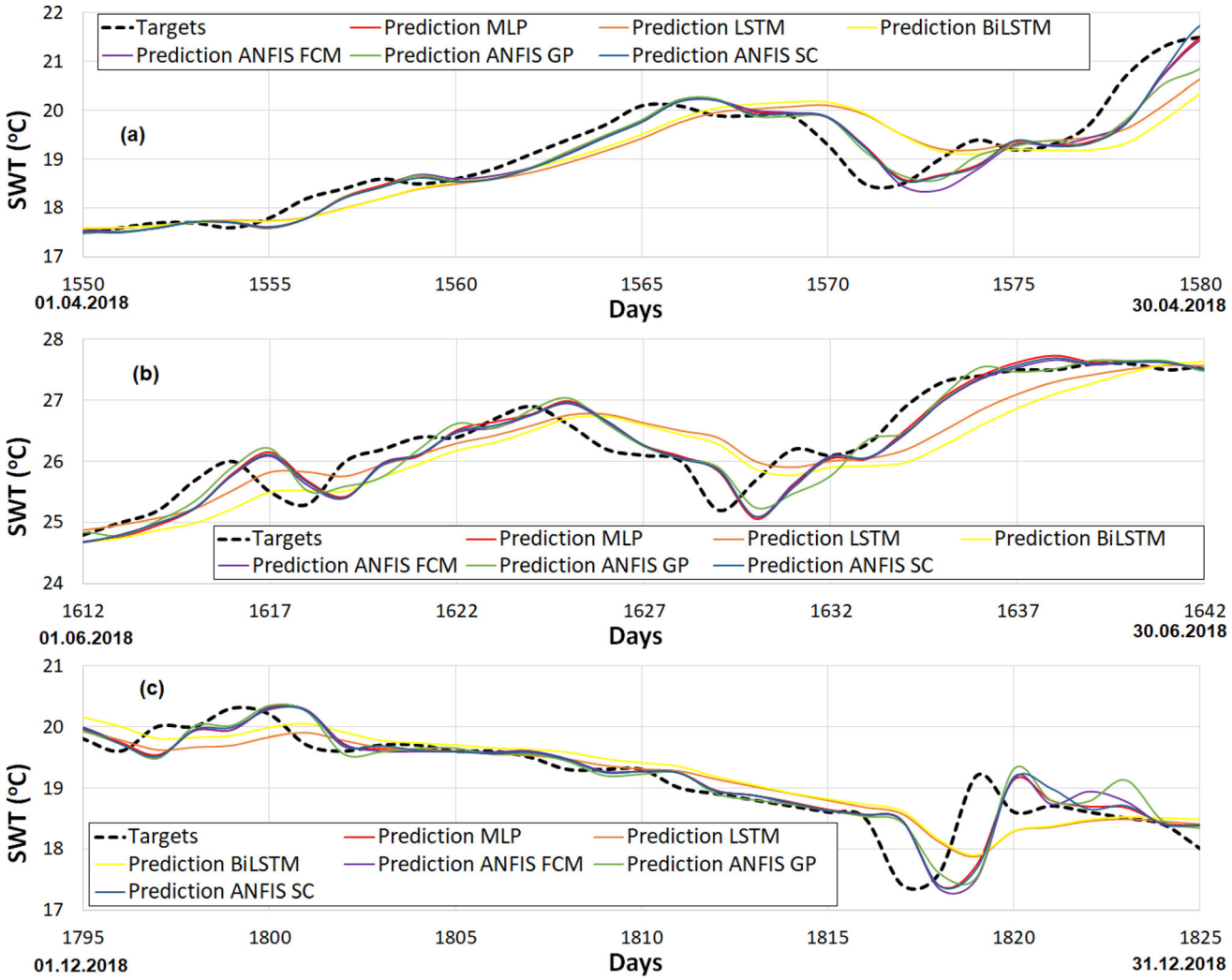

Fig. 15 Daily SWT testing data for Antalya province with targets (dotted lines) and predicted (straight lines) values for one month between (**a**) 01–30 April 2018, (**b**) 01–30 June 2018 and (**c**) 01–31 December 2018

Table 8 Statistical accuracy results of the daily SWT prediction (Best results are in bold)

Method	MAE (°C)	RMSE (°C)	*R*
MLP	0.1886	0.2690	0.99813
LSTM	0.2594	0.3487	0.99688
BiLSTM	0.2880	0.3871	0.99625
ANFIS-FCM	0.1914	0.2741	0.99806
ANFIS-GP	0.1883	0.2696	0.99812
ANFIS-SC	**0.1877**	**0.2683**	**0.99814**

examined for comparison. The estimation using the ANFIS-SC approach yields the most efficient results with an MAE of 0.1877 °C and 0.2683 °C RMSE for Antalya with an *R* value of 0.99814, according to the obtained data in Table 8.

For analyzing the results, the Taylor diagram [56] in Fig. 16 was constructed. A Taylor diagram, as is well known, can be used to assess the accuracy of suggested approaches in several ways. The difference between the points indicating the approaches and the point representing the target value is inversely related to the models' total accuracy to the measured values. Figure 16 demonstrates that the estimations of the ANFIS-SC approach are closer to the observations (targets) than the models. A closer view of the results obtained is placed in the middle of the graph. When the ANFIS-SC technique was utilized, the lowest RMSE value of 0.2683 °C was found. When that approach was utilized, the correlation coefficient (*R*) was close to 99.814 percent. The lowest standard deviation was achieved with BiLSTM, whereas the greatest was achieved using ANFIS-SC.

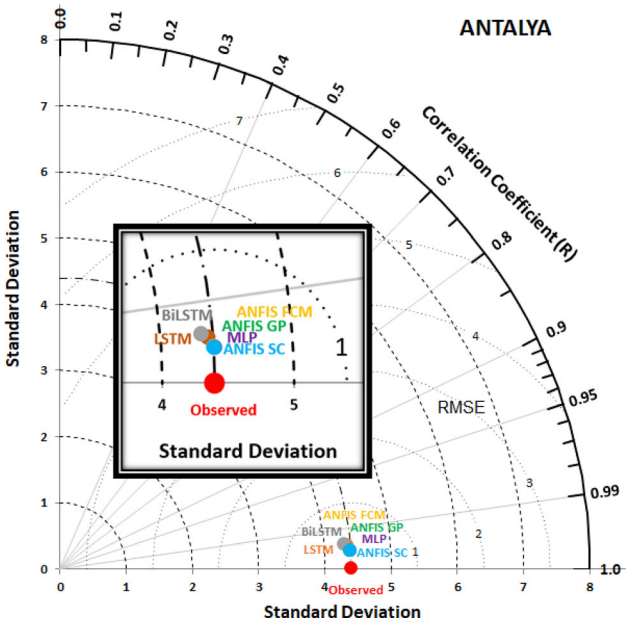

Fig. 16 Taylor diagrams of the proposed models' errors for the test data

6 Conclusion

In this work, the feed-forward artificial neural network (ANN) approach—Multilayer perceptron (MLP), deep learning approaches—the LSTM and BiLSTM neural networks and data-driven approaches—ANFIS-FCM, ANFIS-GP, and ANFIS-SC were utilized to predict 1-day ahead seawater temperature. The Turkish State Meteorological Service measured 5-year daily mean seawater temperatures (SWT) in Antalya province between 2014 and 2018. And these measurements were used as input data for the models. One day ahead SWT may be forecast at any station of time without the need for different meteorological data or complicated calculations with the models offered. The outcomes of all approaches were examined by using different input variables such as neuron number, epoch number, hidden layer number, and influence radius. In addition, the results from all approaches using identical data sets were compared to determine which of the models employed for this study produces more precise results. It was discovered that the ANFIS-SC approach produced exceptional results when the outcomes were analyzed. Different deep learning methods, such as hybrid methods, can be utilized in the future to increase the precision and accuracy of forecast outcomes.

Acknowledgements The author would like to thank the Turkish State Meteorological Service for allowing to use of the seawater temperature data in this research. The author also thanks the office of Scientific Research Projects of Cukurova University for funding this project under Contract no. FBA-2021-14004.

Data availability The datasets generated during and/or analyzed during the current study are available from the corresponding author on reasonable request.

Declarations

Conflict of interest The author(s) declare that they have no known competing financial interests or personal relationships that could have appeared to influence the work reported in this paper.

References

1. Suparta W (2020) Marine heat as a renewable energy source. Widyakala J 7(1):37. https://doi.org/10.36262/widyakala.v7i1.278
2. Teguh NH, Yuliati L, Darmadi DB (2022) Effect of seawater temperature rising to the performance of northern gorontalo small scale power plant. Case Stud Therm Eng 32:101858. https://doi.org/10.1016/j.csite.2022.101858
3. Huang F, Lin J, Zheng B (2019) Effects of thermal discharge from coastal nuclear power plants and thermal power plants on the thermocline characteristics in sea areas with different tidal dynamics. Water 11:2577. https://doi.org/10.3390/w11122577
4. Kisi O, Shiri J (2014) Prediction of long-term monthly air temperature using geographical inputs. Int J Climatol 34:179–186
5. Bilgili M, Sahin B (2010) Prediction of long-term monthly temperature and rainfall in Turkey. Energy Sources Part A Recover Util Environ Eff 32:60–71
6. Zaytar MA, El Amrani C (2016) Sequence to sequence weather forecasting with long short-term memory recurrent neural networks. Int J Comput Appl 143:7–11
7. Tran TKT, Lee T, Shin J-Y, Kim JS, Kamruzzama M (2020) Deep learning-based maximum temperature forecasting assisted with meta-learning for hyperparameter optimization. Atmosphere (Basel) 11:487
8. Roy DS (2020) Forecasting the air temperature at a weather station using deep neural networks. Procedia Comput Sci 178:38–46
9. Ceylan Z (2020) Assessment of agricultural energy consumption of Turkey by MLR and Bayesian optimized SVR and GPR models. J Forecast 39(6):944–956. https://doi.org/10.1002/for.2673
10. Kaytez F (2020) A hybrid approach based on autoregressive integrated moving average and least-square support vector machine for long-term forecasting of net electricity consumption. Energy 197:117200. https://doi.org/10.1016/j.energy.2020.117200
11. Qing X, Niu Y (2018) Hourly day-ahead solar irradiance prediction using weather forecasts by LSTM. Energy 148:461–468. https://doi.org/10.1016/J.Energy.2018.01.177
12. Ozbek A, Yildirim A, Bilgili M (2021) Deep learning approach for one-hour ahead forecasting of energy production in a solar-PV plant. Energy Sources Part A Recov Util Environ Eff. https://doi.org/10.1080/15567036.2021.1924316
13. Ozbek A, Sekertekin A, Bilgili M, Niyazi A (2021) Prediction of 10-Min, hourly, and daily atmospheric air temperature: comparison of LSTM, ANFIS-FCM, and ARMA. Arab J Geosci 14:622. https://doi.org/10.1007/S12517-021-06982-Y
14. Balluff S, Bendfeld J, Krauter S (2015) Short term wind and energy prediction for offshore wind farms using neural networks. In: 2015 international conference on renewable energy research and applications (ICRERA). IEEE, Palermo, pp 379–382. https://doi.org/10.1109/Icrera.2015.7418440

15. Qu X, Xiaoning K, Chao Z (2016) Short-term prediction of wind power based on deep long short-term memory. In: 2016 IEEE Pes Asia-pacific power and energy engineering conference (APPEEC). IEEE, pp 1148–1152
16. Kisi O, Sanikhani H (2015) Modelling long-term monthly temperatures by several data-driven methods using geographical inputs. Int J Climatol 35:3834–3846. https://doi.org/10.1002/Joc.4249
17. Zhang J, Cao X, Xie J, Kou P (2019) An improved long short-term memory model for dam displacement prediction. Math Probl Eng 2019:1–14. https://doi.org/10.1155/2019/6792189
18. Peng L, Liu S, Liu R, Wang L (2018) Effective long short-term memory with differential evolution algorithm for electricity price prediction. Energy 162:1301–1314. https://doi.org/10.1016/J.Energy.2018.05.052
19. Xuan Y, Suixiang S, Lingyu X, Yaya L, Qingsheng M, Miao S (2020) A novel method for sea surface temperature prediction based on deep learning, Math Probl Eng 2020, Article ID 6387173, 9 p. https://doi.org/10.1155/2020/6387173
20. Pravallika MS, Vasavi S, Vighneshwar SP (2022) Prediction of temperature anomaly in Indian Ocean based on autoregressive long short-term memory neural network. Neural Comput Appl 34:7537–7545. https://doi.org/10.1007/s00521-021-06878-8
21. Sarkar P, Janardhan P, Roy P (2020) Prediction of sea surface temperatures using deep learning neural networks. SN Appl Sci 2:1458. https://doi.org/10.1007/s42452-020-03239-3
22. Graf R, Aghelpour P (2021) Daily river water temperature prediction: a comparison between neural network and stochastic techniques. Atmosphere 12(9):1154
23. Zhu S, Nyarko EK, Nyarko MH, Heddam S, Wu S (2019) Assessing the performance of a suite of machine learning models for daily river water temperature prediction. PeerJ 7:e7065. https://doi.org/10.7717/peerj.7065
24. Zhu S, Heddam S, Nyarko EK, Hadzima-Nyarko M, Piccolroaz S, Wu S (2019) Modeling daily water temperature for rivers: comparison between adaptive neuro-fuzzy inference systems and artificial neural networks models. Environ Sci Pollut Res 26(1):402–420
25. Read JS, Jia X, Willard J, Appling AP, Zwart JA, Oliver SK (2019) Process-guided deep learning predictions of lake water temperature. Water Resour Res 55:9173–9190. https://doi.org/10.1029/2019WR024922
26. Rajesh M, Rehana S (2021) Prediction of river water temperature using machine learning algorithms: a tropical river system of India. J Hydroinf 2(3):605–626. https://doi.org/10.2166/hydro.2021.121
27. Feigl M, Lebiedzinski K, Herrnegger M, Schulz K (2021) Machine-learning methods for stream water temperature prediction. Hydrol Earth Syst Sci 25:2951–2977. https://doi.org/10.5194/hess-25-2951-2021
28. Kim BK, Jeong YH (2013) High cooling water temperature effects on design and operational safety of NPPS in the Gulf region nuclear engineering and technology. 45:7 (Technical Note)
29. Aparna SG, D'souza S, Arjun NB (2018) Prediction of daily sea surface temperature using artificial neural networks. Int J Remote Sens 39(12):4214–4231. https://doi.org/10.1080/01431161.2018.1454623
30. Haghbin M, Sharafati A, Motta D et al (2021) Applications of soft computing models for predicting sea surface temperature: a comprehensive review and assessment. Prog Earth Planet Sci 8:4. https://doi.org/10.1186/s40645-020-00400-9
31. Durmayaz A, Sogut OS (2006) Influence of cooling water temperature on the efficiency of a pressurized-water reactor nuclear-power plant. Int J Energy Res 30:799–810. https://doi.org/10.1002/Er.1186
32. Stajkowski S, Kumar D, Samui P, Bonakdari H, Gharabaghi B (2020) Genetic-algorithm-optimized sequential model for water temperature prediction. Sustainability 12(13):5374. https://doi.org/10.3390/su12135374
33. Samadianfard S, Kazemi H, Kisi O, Liu WC (2016) Water temperature prediction in a subtropical subalpine lake using soft computing techniques. Earth Sci Res J 20(2):D1–D11
34. Quan Q, Hao Z, Xifeng H, Jingchun L (2020) Research on water temperature prediction based on improved support vector regression. Neural Comput Appl. https://doi.org/10.1007/s00521-020-04836-4
35. Attia SI (2015) The influence of condenser cooling water temperature on the thermal efficiency of a nuclear power plant. Ann Nucl Energy 80:371–378
36. Darmawan N, Yuwono T (2019) Effect of increasing sea water temperature on performance of steam turbine of Muara Tawar power plant. J Technol Sci 30(2):2088–2033
37. Hey-Min C, Min-Kyu K, Hyun Y (2021) Abnormally high water temperature prediction using LSTM deep learning model. J Intell Fuzzy Syst 40(4):8013–8020
38. Moody J, Darken CJ (1989) Fast learning in networks of locally-tuned processing units. Neural Comput 1:281–294
39. Ding W, Abdullah A, Ahmad A, Payam R, Masoud M, Maria R (2022) Evaluation of the performance of a composite profile at elevated temperatures using finite element and hybrid artificial intelligence techniques. Materials 15(4):1402. https://doi.org/10.3390/ma15041402
40. Hochreiter S, Schmidhuber J (1997) Long short-term memory. Neural Comput 9(8):1735–1780
41. Zahroh S, Hidayat Y, Pontoh RS, Santoso A, Sukono Bon AT (2019) Modeling and forecasting daily temperature in Bandung. In: Proceedings of the international conference on industrial engineering and operations management (November), pp 406–412
42. Salman AG, Heryadi Y, Abdurahman E, Suparta W (2018) Single layer & multi-layer long short-term memory (LSTM) model with intermediate variables for weather forecasting. Procedia Comput Sci 135:89–98
43. Zhang B, Wu JL, Chang PC (2018) A multiple time series-based recurrent neural network for short-term load forecasting. Soft Comput 22(12):4099–4112
44. Liu R, Liu L (2019) Predicting housing price in china based on long short-term memory incorporating modified genetic algorithm. Soft Comput 23(22):11829–11838
45. Schuster M, Paliwal K (1997) Bidirectional recurrent neural networks. IEEE Trans Signal Process 45:2673–2681
46. Graves A, Schmidhuber J (2005) Framewise phoneme classification with bidirectional LSTM networks. In: Proceedings of the 2005 IEEE international joint conference on neural networks, Montreal, QC, Canada, 31 July–4 August, vol 4, pp 2047–2052
47. Zhang A, Lipton ZC, Li M, Smola AJ (2021) Dive into deep learning. arXiv 2021, arXiv:2106.11342.
48. Adytia D, Saepudin D, Pudjaprasetya SR, Husrin S, Sopaheluwakan A (2022) A deep learning approach for wave forecasting based on a spatially correlated wind feature, with a case study in the Java Sea. Indonesia Fluids 7(1):39. https://doi.org/10.3390/fluids7010039
49. Abyaneh HZ, Nia AM, Varkeshi MB, Marofi S, Kisi O (2011) Performance evaluation of ANN and ANFIS models for estimating garlic crop evapotranspiration. J Irrig Drain Eng 137(5):280–286
50. Erduman A (2020) A smart short-term solar power output prediction by artificial neural network. Electr Eng 102(3):1441–1449
51. Benmouiza K, Cheknane A (2019) Clustered ANFIS network using fuzzy c-means, subtractive clustering, and grid partitioning

for hourly solar radiation forecasting. Theoret Appl Climatol 137:31–43
52. Jang JSR (1993) ANFIS: adaptive-network-based fuzzy inference system. IEEE Trans Syst Man Cybern 23(3):665–685. https://doi.org/10.1109/21.256541
53. Karakuş O, Kuruoğlu EE, Altinkaya MA (2017) One-day ahead wind speed/power prediction based on polynomial autoregressive model. IET Renew Power Gener 11(11):1430–1439
54. Mathworks (2020) Fuzzy C-Means Clustering. https://www.mathworks.com/help/deeplearning/ug/long-short-term-memory-networks.html
55. Tabari H, Kisi O, Ezani A, Hosseinzadeh TP (2012) SVM, ANFIS, regression and climate based models for reference evapotranspiration modeling using limited climatic data in a semi-arid highland environment. J Hydrol 444–445:78–89
56. Taylor KE (2001) Summarizing multiple aspects of model performance in a single diagram. J Geophys Res 106:7183–7192. https://doi.org/10.1029/2000JD900719

Publisher's Note Springer Nature remains neutral with regard to jurisdictional claims in published maps and institutional affiliations.

Springer Nature or its licensor (e.g. a society or other partner) holds exclusive rights to this article under a publishing agreement with the author(s) or other rightsholder(s); author self-archiving of the accepted manuscript version of this article is solely governed by the terms of such publishing agreement and applicable law.